

Dynamics of Eddies in the Southeastern Tropical Indian Ocean

F Hanifah¹, N S Ningsih¹, and I Sofian²

¹ Research Group of Oceanography, Faculty of Earth Sciences and Technology,
Bandung Institute of Technology (ITB), Indonesia

² Geospatial Information Agency (BIG), Cibinong, Indonesia

Corresponding author: Farrah Hanifah, E-mail: farrah@oceanography.itb.ac.id

Abstract. A holistic study was done on eddies in the Southeastern Tropical Indian Ocean (SETIO) using the HYbrid Coordinate Ocean Model (HYCOM) for 64 years (from 1950 to 2013). The results from the model were verified against the current and the Sea Surface Height Anomaly (SSHA) from Ocean Surface Current Analyses – Real time (OSCAR) and Archiving, Validation and Interpretation of Satellite Oceanographic Data (AVISO) respectively. The verification showed that the model simulates the condition in the area of study relatively well. We discovered that the local wind was not the only factor that contributed to the formation of eddies in the area. The difference in South Java Current (SJC) flow compared to the Indonesian Throughflow (ITF) and South Equatorial Current (SEC) flow as well as the difference in the relative velocity between the currents in the area led us to suspect that shear velocity may be responsible for the formation of eddies. The results from our model corroborated our prediction about shear velocity. Therefore, we attempted to explain the appearance of eddies in the SETIO based on the concept of shear velocity. By observing and documenting the occurrences of eddies in the area, we found that there are 8 cyclonic and 7 anticyclonic eddies in the SETIO. The distribution and frequency of the appearance of eddies varies, depending on the season.

1. Introduction

The Southeastern Tropical Indian Ocean (SETIO) is the region between the Lesser Sunda Island and the northwestern part of Australia. It is also an area of water mass where the Pacific and the Indian oceans meet (Fieux et al., 1994). Feng and Wijffels (2002), Syamsudin and Kaneko (2013), and Sprintall et al. (1999) found that the dominant currents that always flow through the SETIO are, among others, the Indonesian Throughflow (ITF), the South Java Current (SJC), and the South Equatorial Current (SEC). It was also found that the condition in the SETIO is influenced by a few factors: the local winds and remote forcing, such as the monsoon system (Webster and Fasullo, 2003), the ITF (Gordon et al., 2010; Du and Qu, 2010; Syamsudin and Kaneko, 2013), the SJC (Quadfasel and Cresswell, 1992; Sprintall et al., 1999; Sprintall et al., 2010; Syamsudin and Kaneko, 2013), the SEC (Feng and Wijffels, 2002), eddies (Wyrski, 1962; Cresswell and Golding, 1979; Bray et al., 1997; Yu and Potemra, 2006; Ogata and Matsumoto, 2010; Iskandar et al., 2010), the Rossby waves (Cipollini et al., 2001; Jury and Huang, 2004; Baquero-Bernal and Latif, 2005), the El-Niño Southern Oscillation (ENSO) (Susanto et al., 2001), and the Indian Ocean Dipole (IOD) (Saji et al., 1999; Gualdi et al., 2003).

As mentioned earlier, eddies have been found to influence the condition in the SETIO. It is possible that the presence of this interesting phenomenon may be the reason why the fishing sector thrives in



this area, especially it is part of the Indonesian Regional Management Fisheries (WPP-573 RI). Eddies have important roles in mixing at the ocean surface layer. There are two types of eddies: cyclonic (cold-core) eddies and anticyclonic (warm-core) eddies. Cold-core eddies carry nutrients, which in turn fertilize the ocean's surface layer. This process supports the growth of planktons for biological purposes as reported by Iskandar et al., (2010) in their study on eddies that cause chlorophyll bloom.

In the SETIO, the presence of eddies have been confirmed by Cresswell and Golding (1979), Feng and Wijffels (2002), Yu and Potemra (2006), Ogata and Matsumoto (2010), and Iskandar et al., (2010). In mid-1976, a buoy was released off the west coast of Australia. It propagated towards the SEC and detected eddies that were moving towards the northwest. From the field data, Cresswell and Golding (1979) suspected that eddies that were formed spun in a clockwise direction (cyclonic) with a velocity of about 10 cm/s and a lifespan of two months. Iskandar et al., (2010) confirmed the direction of propagation of the eddy to the west, and further added that they are part of the Rossby waves. Other than cyclonic eddies, there are also anticyclonic eddies that spin in a counter-clockwise direction for southern hemisphere (Griffa et al., 2008). In 1959 and 1960, Wyrtki (1962) detected anticyclonic eddies near the SEC. Moreover, in 1976, Cresswell and Golding (1979) detected that the diameter of the anticyclonic eddies was larger than the diameter of the cyclonic eddies. In addition, other researchers have also detected eddies near the SEC. Bray et al., (1997) detected the presence of an eddies in the SEC south of Java with a lifespan of 60 days based on the sea level data from satellite altimetry combined with the observations on Christmas Island. Feng and Wijffels (2002) also detected eddies in the SEC using TOPEX/Poseidon and ERS-1/ERS-2 satellite altimetry.

This study aims to study the dynamics of eddies in the SETIO by investigating the formation mechanism of eddies, the frequency of appearance, and the distributions of eddies in this area.

2. Data and Methodology

2.1. Data

There were two sets of data used in this study—the data input of the model and the reference data from satellites to verify the model used. For the input to the model, we used the bathymetric data from A 2 minute Elevation Topographic (ETOPO2) (U.S. Department of Commerce, et al., 2006) and map from DISHIDROS TNI-AL (Hydro-Oceanographic Division of Indonesian Navy); the forcing of air temperature; the humidity; the rainfall; the solar radiation and the wind velocity from the National Centers for Environmental Prediction / National Center for Atmospheric Research (NCEP/NCAR) reanalysis data (Kalnay *et al.*, 1996). To verify the model, we used the currents and SSHA from Ocean Surface Current Analyses – Real time (OSCAR), and Archiving, Validation and Interpretation of Satellite Oceanographic Data (AVISO).

2.2. Methodology

In this study, we simulated the conditions of the area studied in this paper using the HYbrid Coordinate Ocean Model (HYCOM) (Bleck, 2002). Simulations were carried out in three steps. Firstly, the model was spun up with climatological data for 20 years. Secondly, the global model (60° S - 60° N and 180° W - 180° E) with a 1/2° resolution was run with real-time forcing input for 64 years (1950-2013). Thirdly, the regional model (21.5° S - 23° N and 90° E - 139° E) with a resolution of 1/8° was nested with real-time forcing input for 64 years (1950-2013). It should be noted that the area that became the focus of this study was the SETIO, with geographic coordinates of 6° S - 16° S and 103° E - 125° E. The global model served to ensure that all factors from outside the investigated area that influenced the conditions in the area of this study were accounted for. The regional model, with better resolution, allowed us to study the focus area more accurately (see figure 1).

The verification was conducted by calculating the bias and Root Mean Square Error (RMSE) of the model and satellites data. The bias and the RMSE were calculated as follows (Chu et al., 2004):

$$\Delta H = H_m(x, y, t) - H_o(x, y, t) \quad (1)$$

$$bias(x, y) = \frac{1}{N} \sum_{i=1}^N \Delta H(x, y, t_i) \quad (2)$$

$$rmse(x, y) = \sqrt{\frac{1}{N} \sum_{i=1}^N [\Delta H(x, y, t_i)]^2} \quad (3)$$

With N , H , H_m , and H_o representing the number of data, the variables used, the variables of the model, and the variables of the observation, respectively.

Once the model was verified, the mechanism that produces eddies was investigated by observing the main currents (ITF, SEC and SJC) in the SETIO. To monitor eddy activity we tracked eddies as closed contour of SSH anomalies and rotation of current then we identified features that displayed the spatial properties of an ocean eddy. The appearance and the distribution of eddies from 1950 to 2013 were documented and analyzed to identify the patterns and the behavior of eddies in this area.

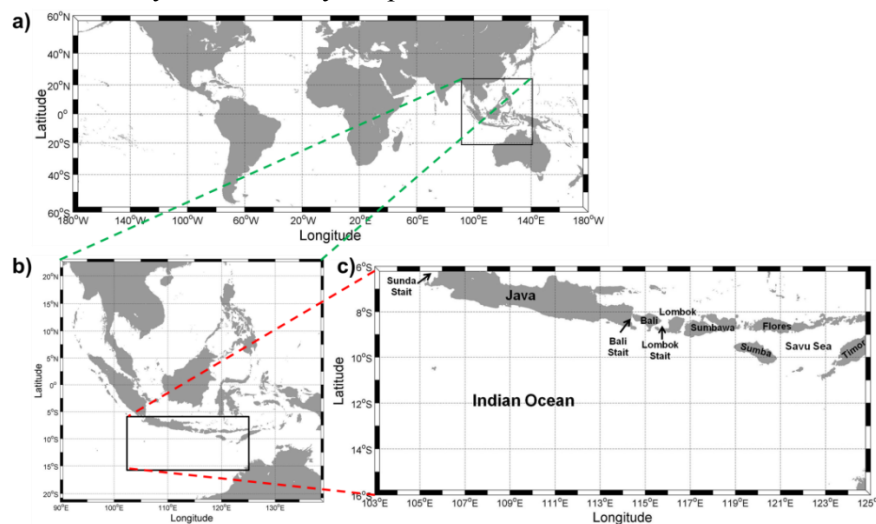


Figure 1. (a) The global model, (b) the regional models, and (c) and study interest area.

3. Results and Discussion

3.1. Verification of Model

Before the model was used in this study, the results produced by the model were verified with satellite data to determine the accuracy. In the verification of currents, it was found that the greatest RMSEs were in points 3 and 4 for the u and v components, respectively; while the smallest were in points 6 for both the u and v components, respectively (figure 2 and Table 1).

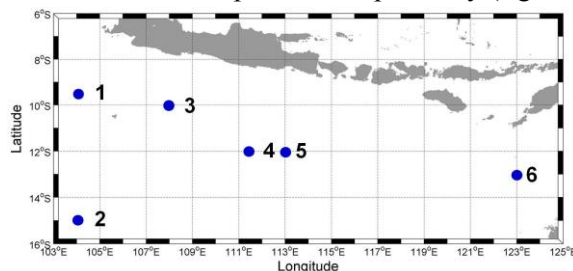


Figure 2. The six points represent the area of study that were used in the verification of the ocean currents.

Table 1. Bias (m/s) and RMSE (m/s) of zonal and meridional current at the points of verification.

Points	1	2	3	4	5	6
RMSE u	0.209	0.141	0.213	0.188	0.147	0.086
RMSE v	0.128	0.094	0.136	0.137	0.131	0.072

From figure 3, the greatest bias was found in the Bali Strait and the southern waters of Sumbawa, while the greatest RMSE was found off of the Java shore at 10° S - 12° S. These occurred most likely because of the different resolutions of the model and AVISO, where the resolution of AVISO was greater ($1/3^{\circ}$ for AVISO compared to $1/8^{\circ}$ for the model). From figure 4, we found that the smallest RMSE (0.036 m) occurred in May, while the largest (0.049 m) occurred in June. In the same figure, it was found that the largest bias (-0.019 m) occurred in June, while the smallest (0 m) occurred in February. Feng and Wijffels (2002) stated that the SEC strengthened during the southeast monsoon season according to the data from the satellite altimetry. Concordantly, from figure 3, the largest RMSE was seen in the area where SEC propagated. The negative value of the bias also means that the value of the data from AVISO were larger than the model results. So, both the bias and the RMSE were the largest during the southeast monsoon season.

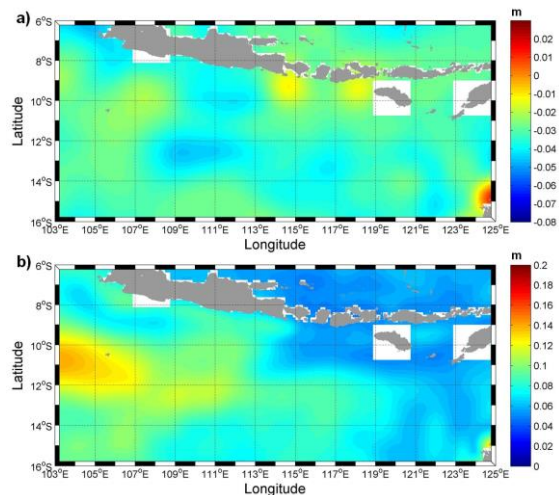


Figure 3. Spatial plot of the average bias (m) (a) and RMSE (m) (b) of SSHA between the model and the reference data (AVISO) from 1993 to 2010.

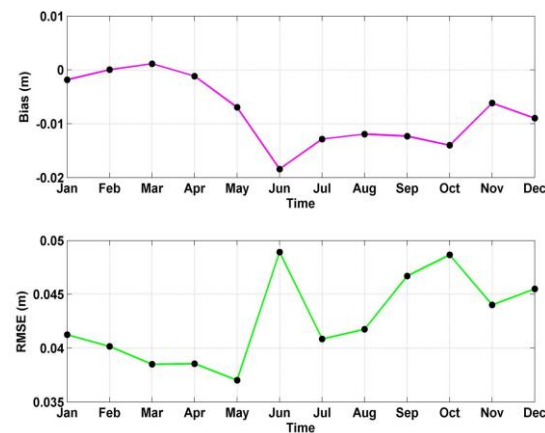


Figure 4. Temporal plot of the monthly average of the bias and RMSE of SSHA between the model and the reference data (AVISO) throughout the area of study.

3.2. General Flow Pattern

We observed the local wind and the currents that flow in this area (figure 5) in order to understand the mechanism that gives rise to the formation of eddies in the SETIO and to determine whether or not the eddies are formed because of the local wind.

Our result (figure 5) shows that SJC appeared only during the transition and northwest monsoon seasons. Particularly during the transition seasons, the SJC was amplified by Kelvin wave that makes its flow strongly towards the east as reported by Molcard *et al.* (2001). On the contrary, during northwest monsoon season, the SJC, which flowed eastward, became weak, causing the SEC to change its directions from westward to eastward by first going to the north. This change in the direction of the flow gave rise to a vortex called eddies. From figure 5, it can also be seen that the current flow pattern did not exactly follow the local wind pattern. This indicates that the flow of the currents in the SETIO was not necessarily influenced by the local wind; there is another force beyond the SETIO called remote forcing, such as SEC, ITF, and SJC that influenced the formation of eddies in this area.

3.3. Shear Velocity and the Formation of Eddies

From figure 5, we found that the SEC and the ITF flowed in opposite directions of the SJC. This observation suggests that shear velocity must have been developed because of the opposite direction of propagation of the currents, which could subsequently give rise to the formation of eddies.

Shear velocity is developed because of the difference in velocity of the currents, when there is a difference in the strength of currents that flow in the same direction (figure 6a) or when the currents flow in opposite directions (figure 6b). Shear velocity give rise to vorticity. In the southern hemisphere, negative vorticity cause clockwise eddy which is followed by the process of divergence, whereas positive vorticity cause anticlockwise eddy, which leads to convergence as shown in figure 6c and figure 6d.

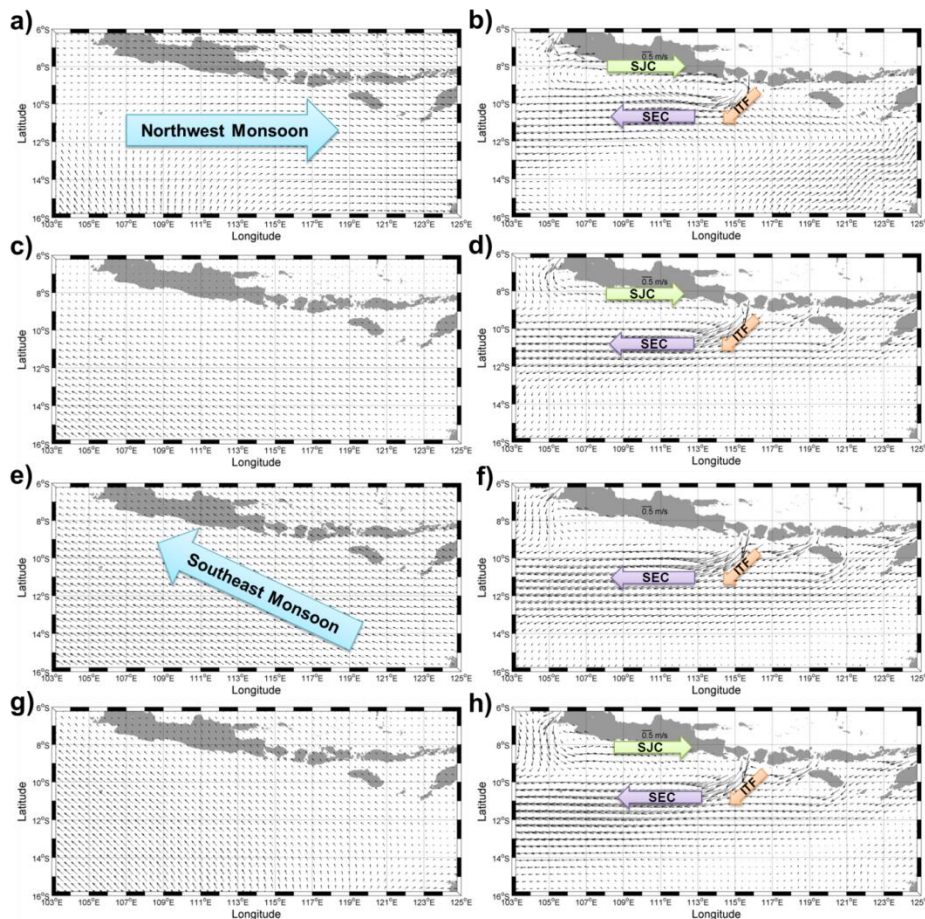


Figure 5. The SETIO local wind (a) and currents flow (b) during northwest monsoon (DJF). The SETIO local wind (c) and currents flow (d) during transitional season 1 (MAM). The SETIO local wind (e) and currents flow (f) during southeast monsoon (JJA). The SETIO local wind (g) and currents flow (h) during transitional season 2 (SON).

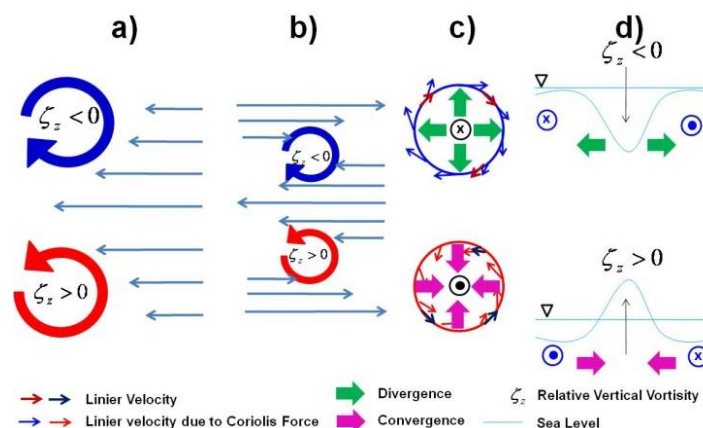


Figure 6. The formation for mechanism of eddies due to shear velocity.

Based on the aforementioned explanation on how a difference in velocity gives rise to shear velocity, each of the major currents in this area (SEC, ITF, and SJC) was studied separately to predict

how each of the currents contributes to the formation of eddies. figure 7a shows that in the case where the SEC flows off shore and the ITF and SJC are not present, there is a difference in the velocity between the SEC and the currents around it. This gives rise to shear velocity, causing the currents around the SEC to spin and form eddies. A cyclonic eddy is expected to form north of the SEC, while an anticyclonic eddy is formed south of the SEC. In the case where only the ITF flows out of the Lombok Strait, shear velocity is also developed because of the difference in the velocity between the ITF and the surrounding currents. This in turn, should cause the formation of a cyclonic eddy west of ITF and an anticyclonic eddy east of ITF (figure 7b). Similarly, shear velocity is also developed during the transition seasons and the northwest monsoon season because of the SJC that flows eastward. As a result, an anticyclonic eddy is expected to form north of SJC near the south coast of Java, while a cyclonic eddy is formed south of SJC (figure 7c).

Collectively, when the three currents (SEC, ITF and SJC) are present, the shear velocity that gives rise to eddy formation is expected to develop because of the difference in the relative velocity between the currents that both flow in the same direction and in opposite direction. Anticyclonic eddies at the south of Lombok Island and at the south of the SEC are formed because of the interaction between SEC and ITF that flow in the same direction. Similarly, anticyclonic eddies near the Java beach are also formed because of the interaction between the SJC and the surrounding currents that flow in the same direction. On the other hand, the shear velocity that occurs as a result of the different flow directions between SEC-ITF and SJC is expected to cause the formation of a cyclonic eddy in the SETIO.

Our prediction based on the observation of shear velocity was that there are two types of eddies in the SETIO (cyclonic and anticyclonic), confirming the findings by Cresswell and Golding (1979) and Wyrski (1962), who detected the presence of cyclonic and anticyclonic eddies in this area, respectively. Moreover, our prediction about the distribution and direction of the eddy rotation in figure 7d also corresponds well to the distribution and direction of the eddy rotation from the model based on 64 years of observation (1950-2013) in figure 8. Thus, shear velocity provides a good explanation for the formation of eddies.

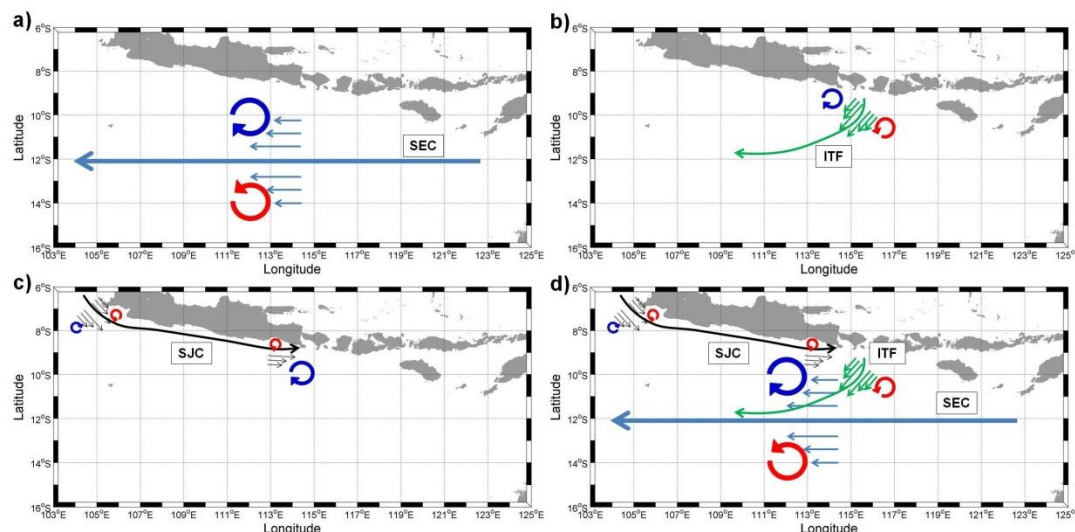


Figure 7. The predicted formation of eddies due to the main currents in the SETIO based on the concept of shear velocity. (a) Formation of eddies due to the SEC, (b) Formation of eddies due to the ITF, (c) Formation of eddies due to the SJC, (d) Formation of eddies due to the interaction of the SEC, the ITF, and the SJC.

With that in mind, we could explain the occurrence of eddies in figure 8 using the concept of shear velocity. figure 8 shows that in the region near the coast of Java, the difference in the velocity of SJC that flowed to the east and the weaker currents around it as well as the morphology of the south coast of Java gave rise to shear velocity. This in turn, produced cyclonic and anticyclonic eddies (C1, A1

and A2). In the north of SEC (between SEC and SJC), there were cyclonic eddies (C2 and C3) due to shear velocity SEC, ITF, and SJC; while in the south of SEC there were anticyclonic eddies (A5, A6 and A7) due to shear velocity, which were caused by the difference in the velocity of SEC and the weaker currents around it. According to the model, the interaction of SEC, ITF, SJC, and other currents can form 8 cyclonic eddy and 7 anticyclonic eddy in total. An A3 eddy is formed because of the difference in the velocity between the ITF that comes out of the Lombok Strait and the weaker currents around it. C4, C6, C7 and C8 eddies are formed because of the presence of eddies that rotate in the opposite direction (anticyclonic eddies A3, A5, A6, and A7) and also because of the difference in the velocity between the anticyclonic eddies and the weaker currents around it. Lastly, C5 and A4 eddies are formed because of the interaction between the currents that pass through the Savu Sea and the morphology of the beaches around it, such as the beaches at Timor Island, Sumba Island, and Flores Island.

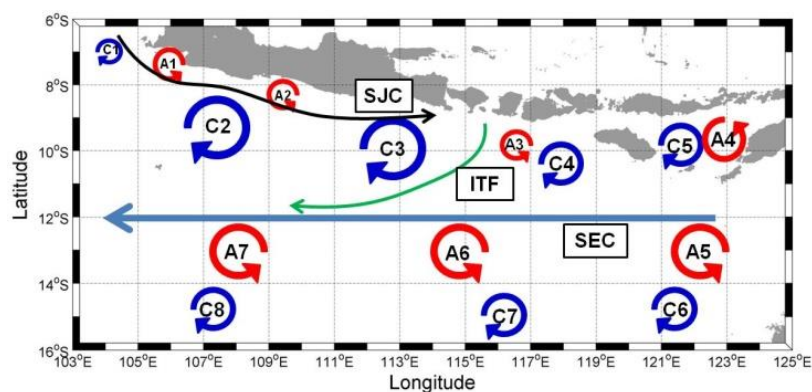


Figure 8. Eddies in the SETIO formed due to the currents (SEC, ITF and SJC) from the model.

3.4. Seasonal Variation of Eddies in the SETIO

Having studied the mechanism of the eddy formation in the SETIO, it is also important to document the number of eddies that are formed in the SETIO and the location of each eddy.

Eddies in the SETIO do not always appear regularly every season. Based on figure 9a, we found that during the northwest monsoon season (DJF), A3 and C5 eddies do not appear. During this period, the ITF is weak, and so an A3 eddy is not formed. In addition, a C5 eddy is not formed because the axis of current flow of the SEC moves offshore, and the SJC, which comes from the western Sumatera coast, flows towards the east. During the 1st transition season (MAM), C5 eddy is not formed (figure 9b). As for the southeast monsoon season, A3, C1, and C5 eddies are not formed (figure 9c) because the current flow axis of the SEC shifts northward towards the Java Island, pushing the SJC towards the west. It is also formed because the ITF strengthens as it moves to the west. Meanwhile during the 2nd transition season (SON), an A4 eddy is not formed (figure 9d).

From figure 10, we also found that the cyclonic eddy that appears most frequently is C3 eddy at the southern part of the east Java coast. Anticyclonic eddies that appears most frequently (figure 11) are: A1 eddy near the Sunda Strait, and eddies (part of Rossby waves) at the south of the SEC (A5, A6 and A7) that flow towards the west. The frequency at which the eddies appear depends on the location at which they are formed. Generally, the cyclonic eddies appear most frequently during the northwest monsoon season (DJF), while the anticyclonic eddies appear most frequently during the 2nd transition season.

4. Conclusion

The verification showed that the model simulates the condition in the area of study relatively well; the errors in the results from the model were relatively small and are within an acceptable range. The difference between the results from the model and the satellite data were mainly caused by the difference in the resolution used. Our results showed that the local wind is not the only force that gives

rise to the formation of eddies in the SETIO. There is another force, called remote forcing, that generates the SEC, the ITF, and the SJC, whose interactions in turn cause the formation of eddies. The difference in the relative velocity of the currents and/or the opposite direction of the flow of the currents develop shear velocity, which in turn forms eddies. This was confirmed by the results produced by the model. We also found that the distribution and the frequency of appearance of eddies varied depending on the season. The observation of the SETIO over 64 years (1950 to 2013) revealed that 8 cyclonic eddies and 7 anticyclonic eddies are formed at different times of the year. During the northwest monsoon season (DJF), there are 7 cyclonic eddies and 6 anticyclonic eddies, while during the 1st transition season (MAM), 7 cyclonic eddies and 7 anticyclonic eddies are formed. During the southeast monsoon season (JJA), 6 cyclonic eddies and 6 anticyclonic eddies are formed, while during the 2nd transition season (SON) 8 cyclonic eddies and 6 anticyclonic eddies are formed. The cyclonic eddy that appears most frequently at the SETIO is the eddy at the southern part of the east Java coast. As for the anticyclonic eddy, the eddies at the south of the SEC that flow towards the west, which are also part of Rossby waves, and the anticyclonic eddy near the Sunda Strait are found to appear most frequently.

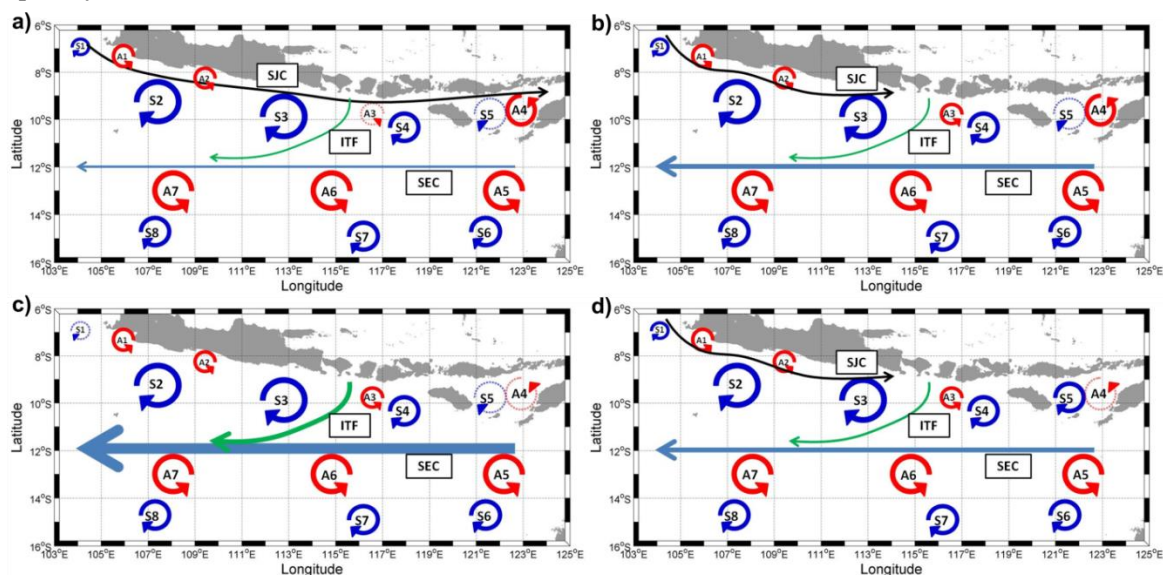


Figure 9. The seasonal distribution of eddies from 64 years of observation during (a) Northwest monsoon (DJF), (b) Transitional season 1 (MAM), (c) Southeast monsoon (JJA), (d) Transitional season 2 (SON).

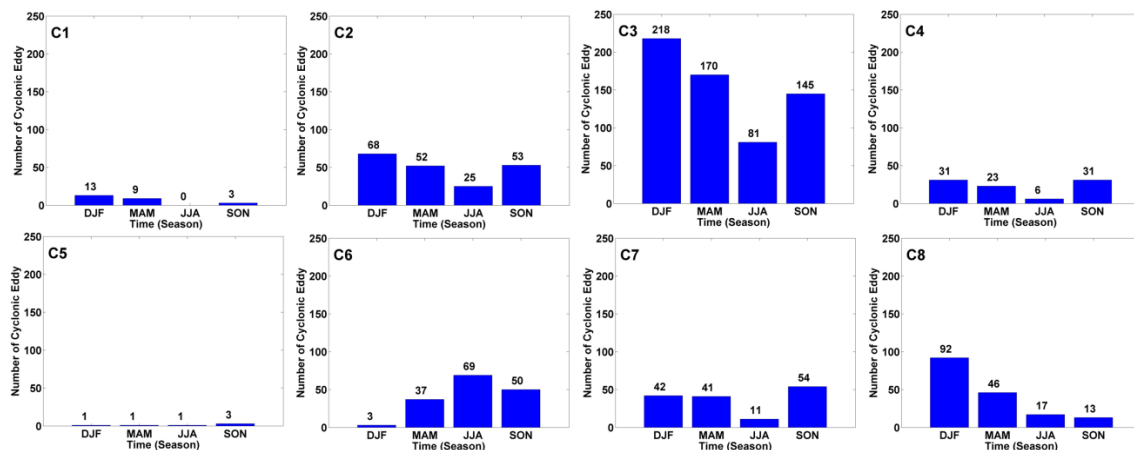


Figure 10. The seasonal frequency of appearance of cyclonic eddies in the SETIO observed over 64 years.

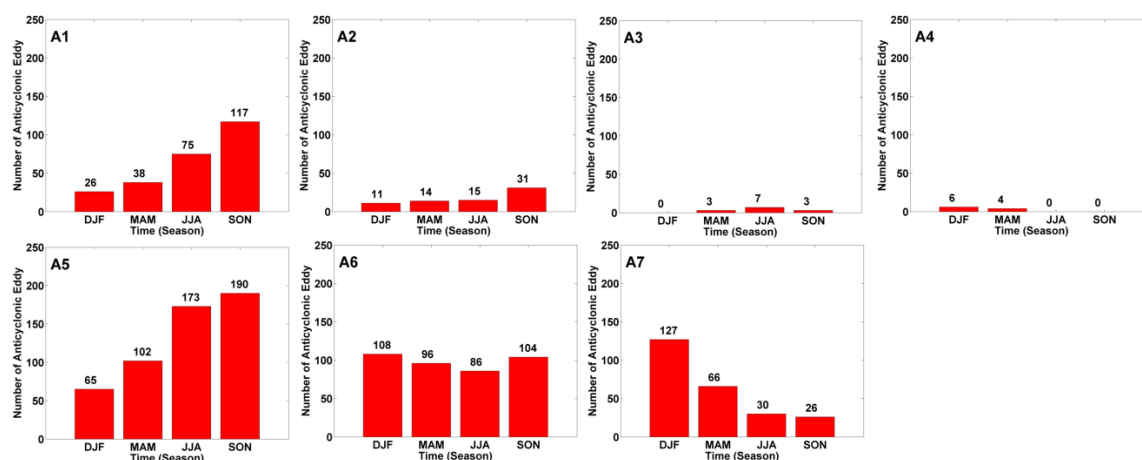


Figure 11. The seasonal frequency of appearance of anticyclonic eddies in the SETIO observed over 64 years.

References

- [1] Baquero-Bernal A and Latif M 2005 Wind-Driven Oceanic Rossby Waves in the Tropical South Indian Ocean with and without an Active ENSO *J. Phys. Oceanogr.* **35**, 729–746
- [2] Bleck R 2002 An oceanic general circulation model framed in hybrid isopycnic-cartesian coordinates *Ocean Modelling* **4**, 55–88
- [3] Bray N A, Wijffels S E, Chong J C, Fieux M, Hautala S, Meyers G and Morawitz W M L 1997 Characteristics of the Indo-Pacific throughflow in the eastern Indian Ocean *Geophys. Res. Lett.* **24**, 2569–2572
- [4] Chu P C, Qi Y, Chen Y, Shi P and Mao Q 2004 South China Sea Wind-Wave Characteristics. Part I: Validation of Wavewatch-III Using TOPEX/Poseidon Data *J. Atmos. Oceanic Tech.* **21**, 1718–1733
- [5] Cipollini P, Cromwell D, Challenor P G and Raffaglio S 2001 Rossby waves detected in global ocean colour data *Geophys. Res. Lett.* **28**(2), 323–326
- [6] Cresswell G R and Golding T J 1979 Satellite-tracked buoy data report III. Indian Ocean 1977 Tasman Sea July to December 1977 *Aust. CSIRO Div. Fish. Oceanogr. Rep.* **101**, 1–44
- [7] Du Y and Qu T 2013 Three inflow pathways of the Indonesian throughflow as seen from the simple ocean data assimilation *Dyn. Atmos. Oceans* **50**, 233–256
- [8] Feng M and Wijffels S 2002 Intraseasonal Variability in the South Equatorial Current of the East Indian Ocean *J. Phys. Oceanogr.* **32**, 265–277
- [9] Fieux M, Andrieu C, Delecluse P, Ilahude A G, Kartavtseff A, Mantisi F, Molcard R and Swallow J C 1994 Measurements within the Pacific-Indian Oceans Throughflow region *Deep Sea Res. Part I* **41**, 1091–1130
- [10] Gordon A L, Sprintall J, Van Aken H M, Susanto D, Wijffels S, Molcard R, Field A, Pranowo W and Wirasantosa S 2010 The Indonesian throughflow during 2004–2006 as observed by the INSTANT program *Dyn. Atmos. Oceans* **50**, 115–128
- [11] Griffa A, Lumpkin R and Veneziani M 2008 Cyclonic and anticyclonic motion in the upper ocean *Geophys. Res. Lett.* **35**(L01608), 1–5
- [12] Gualdi S, Guilyardi E, Navarra A, Masina S and Delecluse P 2003 The interannual variability in the tropical Indian Ocean as simulated by a CGCM *Clim. Dyn.* **20**, 567–582
- [13] Iskandar I, Sasaki H, Sasai Y, Masumoto Y and Mizuno K 2010 A numerical investigation of eddy-induced chlorophyll bloom in the southeastern tropical Indian Ocean during Indian Ocean Dipole—2006 *Ocean Dyn.* **60**, 731–742

- [14] Jury M R and Huang B 2004 The Rossby wave as a key mechanism of Indian Ocean climate variability *Deep Sea Res. Part I* **51**, 2123–2136
- [15] Kalnay E, Kanamitsu M, Kistler R, Collins W, Deaven D, Gandin L, Iredell M, Saha S, White G, Woolen J, Zhu Y, Chelliah M, Ebisuzaki W, Higgins W, Janowiak J, Mo K C, Ropelewski C, Wang J, Leetma A, Reynolds R, Jenne R, Joseph D 1996 The NCEP/NCAR 40-year reanalysis project *Bull. Amer. Meteor. Soc.* **77**, 437-471
- [16] Molcard R M, Fieux M and Syamsudin F 2001 The throughflow within Ombai Strait *Deep Sea Res.* **48**, 1237-1253
- [17] Ogata T and Matsumoto Y 2010 Interactions between mesoscale eddy variability and Indian Ocean dipole events in the Southeastern tropical Indian Ocean—case studies for 1994 and 1997/1998 *Ocean Dyn.* **60**, 717–730
- [18] Quadfasel D and Cresswell G R 1992 A Note on the Seasonal Variability of the South Java Current *J. Geophys. Res.* **97**(C3), 3685-3688
- [19] Saji N H, Goswami B N, Vinayachandran P N and Yamagata T 1999 A dipole mode in the tropical Indian Ocean *Nature* **401**, 360–363
- [20] Sprintall J, Chong J, Syamsudin F, Morawitz M, Hautala S, Bray N and Wijffels S 1999 Dynamics of the South Java Current in the Indo-Australian Basin *Geophys. Res. Lett.* **26**(16), 2493-2496
- [21] Sprintall J, Wijffels S, Molcard R and Jaya I 2010 Direct evidence of the South Java Current system in Ombai Strait *Dyn. Atmos. Oceans* **50**, 140–156
- [22] Susanto R D, Gordon A L and Zheng Q 2001 Upwelling along the Coast of Java and Sumatra and its Relation to ENSO *Geophys. Res. Lett.* **28**(8), 1599-1602
- [23] Syamsudin F and Kaneko A 2013 Ocean variability along the southern coast of Java and Lesser Sunda Islands *J. Oceanogr.*
- [24] U.S. Department of Commerce, National Oceanic and Atmospheric Administration, National Geophysical Data Center 2006 2-minute Gridded Global Relief Data (ETOPO2v2) <http://www.ngdc.noaa.gov/mgg/fliers/06mgg01.html>
- [25] Webster P J and Fasullo J 2003 Monsoon: Dynamical Theory in *Encyclopedia of Atmospheric Sciences*. Eds. J. Holton and J. A. Curry. Academic Press, 1370-1385
- [26] Wyrtki K 1962 The upwelling in the region between Java and Australia during the Southeast Monsoon *Aust. J. Mar. Freshwat. Res.* **17**, 217-225
- [27] Yu Z and Potemra J 2006 Generation mechanism for the intraseasonal variability in the Indo-Australian basin *J. Geophys. Res.*, **111**, C02013